Proton–proton Overhauser NMR spectroscopy with polypeptide chains in large structures

Reto Horst*†, Gerhard Wider*, Jocelyne Fiaux*‡, Eric B. Bertelsen§¶, Arthur L. Horwich†§, and Kurt Wüthrich*†‖

*Institut für Molekularbiologie und Biophysik, Eidgenössische Technische Hochschule Zürich, CH-8093 Zürich, Switzerland; §Howard Hughes Medical Institute and Department of Genetics, Yale University School of Medicine, New Haven, CT 06510; and †Department of Molecular Biology, The Scripps Research Institute, La Jolla, CA 92037

Contributed by Kurt Wüthrich, August 21, 2006

The use of ^{1}H–^{1}H nuclear Overhauser effects (NOE) for structural studies of uniformly deuterated polypeptide chains in large structures is investigated by model calculations and NMR experiments. Detailed analysis of the evolution of the magnetization during ^{1}H–^{1}H NOE experiments under slow-motion conditions shows that the maximal ^{1}H–^{1}H NOE transfer is independent of the overall rotational correlation time, even in the presence of chemical exchange with the bulk water, provided that the mixing time is adjusted for the size of the structure studied. ^{1}H–^{1}H NOE buildup measurements were performed for the 472-kDa complex of the 72-kDa cochaperonin GroES with a 400-kDa single-ring variant of the chaperonin GroEL (SR1). These experiments demonstrate that multidimensional NOESY experiments with cross-correlated relaxation-enhanced polarization transfer and transverse relaxation-optimized spectroscopy elements can be applied to structures of molecular masses up to several hundred kilodaltabs, which opens new possibilities for studying functional interactions in large maromolecular assemblies in solution.

^{1}H–^{1}H NOE | GroE chaperonine system | NMR assignments | protein structure

Resonance assignments in the NMR spectra of uniformly ^{2}H,^{13}C,^{15}N-labeled proteins in structures with molecular sizes up to ≈150–250 kDa have been obtained from transverse relaxation-optimized spectroscopy (TROSY)-type triple-resonance experiments, which use heteronuclear through-bond scalar coupling connectivities for sequential assignment of the backbone $^1H^N$, ^{15}N, $^{13}C^\alpha$, and ^{13}CO resonances (1–7). With larger molecular sizes, these experiments deteriorate because of signal loss by fast transverse relaxation. For example, the efficiency of the magnetization transfer from ^{15}N to ^{13}CO and back has been measured to be between 0.1 and 0.003 for individual dipeptide segments in the 110-kDa 7,8-dihydroneopterin aldolase (DHNA) from *Staphyloccocus aureus* (8), and model calculations predict that the transfer efficiency would be >10 times smaller for proteins >500 kDa. Here, we explore the use of ^{1}H–^{1}H nuclear Overhauser spectroscopy (NOESY) (9, 10) in large molecular structures not only as an alternative to triple-resonance experiments for detecting sequential connectivities that can yield resonance assignments (11–13), but also for identification of long-range NOEs for the characterization of the protein conformation.

In its practical applications, this work is a follow-up of NMR studies with correlation experiments of uniformly ^{15}N,^{2}H-labeled GroES in 1:1 complexes with the unlabeled 800-kDa chaperonin GroEL and its 400-kDa single-ring variant SR1, where tentative resonance assignments for GroEL-bound GroES were derived from chemical shift comparisons with free GroES (14). Although most of the amino acids of GroES have nearly identical shifts for the protein free in solution or in the complex with the chaperonin, several cross-peaks in chaperonin-bound GroES could not be correlated with any of the peaks of free GroES. These so far unassigned amino acids are of special interest, because they form a polypeptide segment that mediates contacts with the GroEL apical domains (15–18). Here, a 3D ^{15}N-resolved [^{1}H,^{1}H]-NOESY experiment using TROSY, cross-correlated relaxation-induced polarization transfer (CRIPT), and cross-correlated relaxation-enhanced polarization transfer (CRINEPT) elements has been developed for ^{1}H–^{1}H NOE measurements in large structures, and is applied to the 470-kDa complex of ^{2}H,^{15}N-labeled GroES bound to SR1 to obtain assignments for these largely shifted resonances and to investigate long-range ^{1}H–^{1}H NOEs that provide previously unreported structural information on GroES in the chaperonin.

Results and Discussion

We first describe model calculations used to explore the behavior of ^{1}H–^{1}H NOEs in large deuterated proteins in H_2O solution in the presence of chemical exchange of protons with the solvent. The assumptions made in these calculations are described, and otherwise the simulations were based on the known molecular coordinates of the proteins considered, in particular the interproton distances in DHNA and GroES were derived from the crystal structure coordinates (18, 19). The rotational correlation times, τ_c, of the protein DHNA and of the 1:1 complexes GroES/SR1 and GroES/GroEL in aqueous solution were chosen to have values of 100, 185, and 350 ns, respectively. These τ_c values were chosen to enable a direct comparison of the model calculations with experimental [^{1}H,^{1}H]-NOE data. The results from the model calculations were then used to optimize the setup of NOESY experiments with the GroES/SR1 complex, and the predictions from the simulations are compared with experimental measurements.

Modeling the ^{1}H–^{1}H NOE-Buildup in Uniformly Deuterated Proteins in H_2O Solution. Because water protons can undergo chemical exchange with oxygen- or nitrogen-bound protons of the protein, bulk water magnetization is transferred to the protein via this exchange mechanism (20). In large structures, spin diffusion efficiently transfers this magnetization further to nonexchangeable hydrogen protons (21). Therefore, chemical exchange with the bulk water needs to be considered in model calculations of ^{1}H–^{1}H NOE buildup curves. Here, we assume that all carbon-bound hydrogen positions in a protein are occupied by ^{2}H and that all nitrogen- and oxygen-bound hydrogen positions contain

Author contributions: R.H., G.W., A.L.H., and K.W. designed research; R.H. and J.F. performed research; J.F., E.B.B., and A.L.H. contributed new reagents/analytic tools; R.H. analyzed data; and R.H. and G.W. wrote the paper.

The authors declare no conflict of interest.

Abbreviations: CRINEPT, cross-correlated relaxation-enhanced polarization transfer; CRIPT, cross-correlated relaxation-induced polarization transfer; DHNA, 7,8-dihydroneopterin aldolase; HMQC, heteronuclear multiple-quantum spectroscopy; TROSY, transverse relaxation-optimized spectroscopy.

‡Present address: Zentrum für Molekularbiologie der Universität Heidelberg, D-69120 Heidelberg, Germany.

¶Present address: Biophysics Research Division, University of Michigan, Ann Arbor, MI 48109-1042.

‖To whom correspondence should be addressed. E-mail: wuthrich@scripps.edu.

^{1}H, so that the hydrogen atoms in the system then belong to one of three classes: A, B, or W (21). Class A contains those protein protons that exchange sufficiently slowly to have resonance lines that are separated from the water resonance, i.e., backbone and side chain amide protons. For the present treatment, these class A protons are assumed to be stably bound to the attached heavy atom ("nonexchanging"). Class B consists of the protein protons that are in fast exchange with the bulk water and resonate at the water frequency, i.e., all hydroxyl protons and the nitrogen-bound side chain protons of Lys and Arg (class B would also include protons of internal water molecules, but the crystal structures of the proteins used for this study do not include any protons from such "structural waters"). Class W contains the bulk water protons. The total number of class A and B protons is given by n_A and n_B, respectively. The time evolution of ^{1}H–^{1}H NOEs in such systems with chemical exchange can be described by the following set of coupled linear differential equations (21–24):

$$\frac{d}{dt}\begin{pmatrix}\boldsymbol{\eta}_{A,t}\\ \boldsymbol{\eta}_{B,t}\\ \eta_{W,t}\end{pmatrix} = -\left\{\begin{bmatrix}\mathbf{R}_A & \mathbf{R}_{AB} & \mathbf{0}\\ \mathbf{R}_{AB}^{\mathrm{T}} & \mathbf{R}_B & \mathbf{0}\\ \mathbf{0} & \mathbf{0} & \rho_{\mathrm{W}}\end{bmatrix} + \begin{bmatrix}\mathbf{0} & \mathbf{0} & \mathbf{0}\\ \mathbf{0} & \mathbf{K}_B & -\boldsymbol{\kappa}_W\\ \mathbf{0} & -\boldsymbol{\kappa}_B^{\mathrm{T}} & k_W\end{bmatrix}\right\}\cdot\begin{bmatrix}\boldsymbol{\eta}_{A,t}\\ \boldsymbol{\eta}_{B,t}\\ \boldsymbol{\eta}_{W,t}\end{bmatrix}. \quad [1]$$

$\boldsymbol{\eta}_{A,t}$ and $\boldsymbol{\eta}_{B,t}$ are vectors with n_A and n_B components, respectively, describing the NOE for the nonexchanging protein protons A and the exchanging protein protons B at time t. $\eta_{W,t}$ denotes the NOE for the water protons at time t. ρ_W is the longitudinal relaxation rate of the water protons. $\mathbf{R}_A$, $\mathbf{R}_B$, and $\mathbf{R}_{AB}$ are relaxation submatrices with dimensions $n_A \times n_A$, $n_B \times n_B$, and $n_B \times n_A$, respectively, which describe the dipolar relaxation of the spin system. The coefficients of these matrices are given by Eqs. **2** and **3** (24)

$$\mathbf{R}_{X,ii} = \alpha_H \sum_j r_{ij}^{-6}(3J_1 + 6J_2 + J_0),\ X \in \{A, B\} \quad [2]$$

$$\mathbf{R}_{X,ij} = -\alpha_H r_{ij}^{-6}(6J_2 - J_0),\ X \in \{A, B, AB\}. \quad [3]$$

r_{ij} is the distance between the spins i and j, $\alpha_H = 5.6965 \times 10^{10}$ Å s^{-2} is the ^{1}H–^{1}H dipolar interaction constant, and $J_m = 2\tau_c/5(1 + n^2\omega_{ij}^2\tau_c^2)$ are the spectral density functions, which depend on the frequencies ω_{ij} of the transitions that are relevant for the relaxation process, and on the effective correlation time τ_c for the interacting proton pair. For large molecular sizes at high magnetic fields, one reaches the "spin diffusion limit" where only J_0 needs to be considered, with $J_0 = 2\tau_c/5$ for isotropic rotational tumbling. Longitudinal cross-correlated relaxation (25, 26) and chemical shift anisotropy relaxation make negligibly small contributions to the overall longitudinal ^{1}H relaxation rates under the conditions relevant for the present study, and their contributions are therefore not considered in Eqs. **2** and **3**. $\mathbf{K}_B$ stands for the $n_B \times n_B$-dimensional kinetic matrix, and the two n_B-dimensional vectors $\boldsymbol{\kappa}_B$ and $\boldsymbol{\kappa}_W$ describe the effects from chemical exchange. Their coefficients are given by $\mathbf{K}_{B,ij} = \delta_{ij}\tau_{b,i}^{-1}$, $\kappa_{B,i} = \tau_{B,i}^{-1}$, and $\boldsymbol{\kappa}_{W,i} = (n_B\tau_W)^{-1}$ (23), and $k_W = \tau_W^{-1}$. $\tau_{B,i}$ and τ_W are the average residence times of a proton in the protein site i, and in the bulk water, respectively. For all class B hydrogens (see above), the residence times in the protein sites are of the same order of magnitude at physiological pH. Thus, for all positions i, there is a common intrinsic exchange rate, $k_B \equiv \tau_{B,i}^{-1}$.

In the presently used NOESY experiments (see *Materials and Methods*), the water magnetization is flipped back to the positive z axis to avoid saturation of the protein protons via chemical exchange (27). Therefore, the water magnetization is in thermal equilibrium during the mixing time, so that to a good approximation $\eta_W = 0$. Because the total bulk water proton concentration is ≈100,000-fold larger than that of individual protein protons, the evolution of the protein magnetization does not measurably influence the magnetization state of the bulk water, and hence Eq. **1** simplifies to the form Eq. **4**:

$$\frac{d}{dt}\begin{pmatrix}\boldsymbol{\eta}_{A,t}\\ \boldsymbol{\eta}_{B,t}\end{pmatrix} = -\begin{bmatrix}\mathbf{R}_A & \mathbf{R}_{AB}\\ \mathbf{R}_{AB}^{\mathrm{T}} & \mathbf{R}_B + \mathbf{K}_B\end{bmatrix}\cdot\begin{pmatrix}\boldsymbol{\eta}_{A,t}\\ \boldsymbol{\eta}_{B,t}\end{pmatrix} = -\mathbf{D}\cdot\begin{pmatrix}\boldsymbol{\eta}_{A,t}\\ \boldsymbol{\eta}_{B,t}\end{pmatrix}. \quad [4]$$

The solution of Eq. **4** is given by **5**, where **D** is the dynamic matrix, and τ_m is the NOESY mixing time:

$$\begin{pmatrix}\boldsymbol{\eta}_{A,\tau_{\mathrm{m}}}\\ \boldsymbol{\eta}_{B,\tau_m}\end{pmatrix} = \exp\{-\mathbf{D}\tau_m\}\cdot\begin{pmatrix}\boldsymbol{\eta}_{A,0}\\ \boldsymbol{\eta}_{B,0}\end{pmatrix}. \quad [5]$$

The cross-peak volume between two resonances i and j in a 2D [^{1}H,^{1}H]-NOESY experiment with mixing time τ_m, $\mathbf{a}_{ij}(\tau_m)$ is given by the NOE matrix **6** (28)

$$\mathbf{a}_{ij}(\tau_m) = \exp\{-\mathbf{D}\tau_m\}_{ij}. \quad [6]$$

Even though Eq. **6** has to be solved numerically to describe the evolution of a spin system during the NOESY mixing time (see below), some simple rules for systems with protons in fast exchange with the bulk water ($k_B > \max(\mathbf{R}_{B,ii})$) can be derived. For example, if the exchange terms are dominant over the relaxation terms for the exchanging protons, the τ_m dependence of the NOE enhancements for class B protons can be described by Eq. **7**:

$$\boldsymbol{\eta}_{B,\tau_m} = \exp\{-\mathbf{K}_B\tau_m\}\cdot\boldsymbol{\eta}_{B,0}. \quad [7]$$

Applying the method of variation of constants (29) to Eqs. **4** and **7** leads to Eq. **8** for $\boldsymbol{\eta}_{A,\tau_m}$

$$\boldsymbol{\eta}_{A,\tau_m} = \exp\{-\mathbf{R}_A\tau_m\}\cdot\boldsymbol{\eta}_{A,0} + (k_B\mathbf{E}_A - \mathbf{R}_A)^{-1}\cdot\mathbf{R}_{AB} \times \exp\{-\mathbf{K}_B\tau_m\}\cdot\boldsymbol{\eta}_{B,0}. \quad [8]$$

$\mathbf{E}_A$ is the $n_{\mathrm{A}} \times n_{\mathrm{A}}$-dimensional unity matrix. The second term on the right side of Eq. **8** vanishes if k_B is large compared with the coefficients of $\mathbf{R}_A$ and $\mathbf{R}_{AB}$ or if $\mathbf{R}_{AB} \approx 0$; i.e., if the interactions between the nonexchanging group A protons and the rapidly exchanging group B protons are weak. In both situations, the contribution from the chemical exchange of protons is negligibly small, so that the Eq. **8** simplifies to the form of Eq. **9**:

$$\boldsymbol{\eta}_{A,\tau_m} = \exp\{-\mathbf{R}_A\tau_m\}\cdot\boldsymbol{\eta}_{A,0}. \quad [9]$$

The NOESY cross-peak volumes between pairs of amide protons (defined in Eq. **6**) are then given by Eq. **10**:

$$\mathbf{a}_{ij}(\tau_m) = \exp\{-\mathbf{R}_A\tau_m\}_{ij}. \quad [10]$$

Two key parameters for the description of the NOE are the maximal magnetization transfer between two spins i and j, $\mathbf{a}_{ij}^{\max}$, and the corresponding optimal mixing time, τ_m^o

$$\mathbf{a}_{ij}(\tau_m^o) = \mathbf{a}_{ij}^{\max}. \quad [11]$$

In the spin diffusion limit, $\mathbf{R}_A$ depends linearly on the rotational correlation time τ_c, with $J_0 = 2\tau_c/5$ and $J_1 = J_2 = 0$ (Eqs. **2** and **3**). The exponent in Eq. **10** then becomes proportional to the product of τ_c and τ_m, so that τ_m^o is inversely proportional to τ_c. The maximal achievable NOE, $\mathbf{a}_{ij}^{\max}$, is thus independent of the size of the protein, provided that τ_m is properly adjusted to the size.

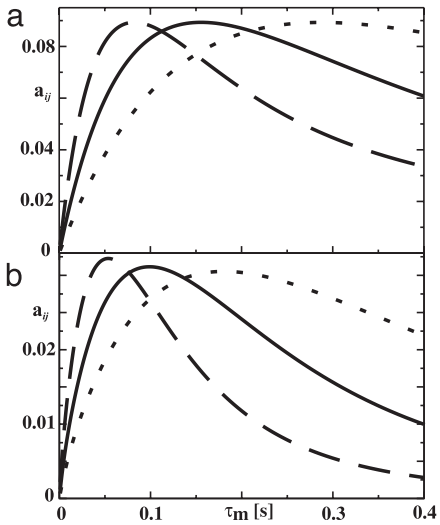

Fig. 1. Plots of simulated NOE cross peak intensities, $\mathbf{a}_{ij}(\tau_m)$, versus the mixing time τ_m (Eq. **6**). The atom coordinates of all backbone amide protons and the exchangeable side chain protons of one subunit of GroES were used for the calculation, as described in *Materials and Methods*. Three different, effective rotational correlation times are considered, i.e., $\tau_c = 100$ ns (dotted line), 185 ns (solid line), and 350 ns (dashed line), where $\tau_c = 185$ and 350 ns are estimates for the GroES complexes with SR1 and GroEL, respectively. For the side chain hydroxyl protons of Ser, Thr, and Tyr, and the side chain ^{15}N-bound protons of Arg and Lys, the exchange rate was set to 150 s^{-1} (49). (*a*) $\mathbf{a}_{ij}(\tau_m)$ for the amide proton pair of V43 and G44, which has only weak exchange contributions, because the two atoms are separated by 4.3 Å, and both hydrogens are >8.0 Å from the nearest rapidly exchanging proton. (*b*) $\mathbf{a}_{ij}(\tau_m)$ for the amide proton pair of S35 and T36, which has strong exchange effects, because the two atoms are separated from each other by 4.5 Å, and both amide protons are close to their side chain hydroxyl groups.

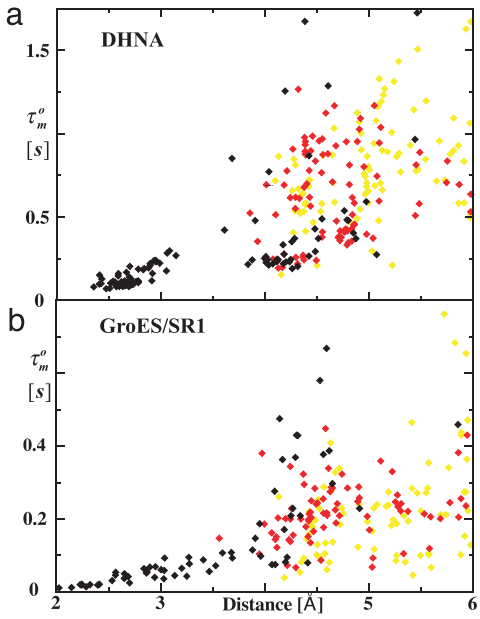

Fig. 2. Optimal mixing time, τ_m^o, for pairs of backbone amide protons plotted versus the ^{1}H–^{1}H distance. The distances between the amide protons were calculated from the crystal structures, as described in *Materials and Methods*. The data were calculated with Eqs. **11** and **12**. (*a*) τ_m^o for proton pairs in one subunit of DHNA, calculated with $\tau_c = 45$ ns (50). (*b*) τ_m^o for proton pairs in one subunit of GroES in the complex with SR1, calculated with $\tau_c = 185$ ns (51). The data points are color-coded according to the optimal transfer efficiencies (Eq. **11**): black, $\mathbf{a}_{ij}^{max} > 0.1$; red, $\mathbf{a}_{ij}^{max} > 0.05$; yellow, $\mathbf{a}_{ij}^{max} \leq 0.05$.

Numerical ^{1}H–^{1}H-NOE Simulations. ^{1}H–^{1}H-NOE buildup calculations were performed by using a matrix diagonalization scheme that is described in *Materials and Methods*. Fig. 1 presents calculated NOESY buildup curves of two different pairs of "group A" backbone amide protons in GroES, i.e., V43/G44 (distance, 4.3 Å) and S35/T36 (distance, 4.5 Å). The amide protons of V43 and G44 are >8.0 Å apart from the nearest water protons or fast exchanging protein hydrogens, and the contributions from exchanging "group B" protons are therefore weak. In contrast, the backbone amide protons of S35 and T36 are within 5.0 Å of their respective side chain hydroxyl protons. For both spin pairs, the maximal transfers, $\mathbf{a}_{ij}^{max}$ (Eq. **11**), are nearly independent of the correlation time, with $\mathbf{a}_{ij}^{max}$ for V43/G44 increasing by <1% when going from $\tau_c = 100$ ns to $\tau_c = 350$ ns (Fig. 1*a*). For S35/T36, $\mathbf{a}_{ij}^{max}$ differs by only ≈10% over the same τ_c range, despite the strong exchange contribution (Fig. 1*b*). These results confirm the previous qualitative interpretation of Eq. **10**, that $\mathbf{a}_{ij}^{max}$ for spin pairs with weak interactions to exchangeable hydrogen protons is independent of τ_c for macromolecular structures beyond 100 kDa, provided that the mixing time τ_m of the NOESY experiment is adjusted close to the optimal mixing time, τ_m^o, for the particle size studied.

The sensitivity loss in NOESY experiments of high molecular weight systems due to efficient transverse relaxation requires the NOE transfer efficiency to be maximized by using optimal mixing times τ_m^o (Eq. **11**). For DHNA, and for GroES in the GroES/SR1 complex, values for τ_m^o were calculated for all pairs of amide protons separated by <6.0 Å (Fig. 2). The color coding of the data points in Fig. 2 reflects the $\mathbf{a}_{ij}^{max}$ values. For internuclear distances <4.0 Å, the optimal mixing times have average values of ≈120 ms for DHNA ($\tau_c = 45$ ns) and 75 ms for the GroES/SR1 complex ($\tau_c = 185$ ns), and the maximal transfer efficiencies are >0.1 (black diamonds). In DHNA, most of these NOEs can be attributed to $d_{NN}(i,i+1)$ distances in α-helices, based on the previous resonance assignments (4); these distances have a length of ≈2.8 Å (11, 19). For internuclear distances >3.5 Å, the maximal transfer efficiencies as well as the optimal mixing times are widely dispersed for both structures, which reflects that for larger interproton distances, "spin diffusion" via other protons becomes an increasingly efficient magnetization transfer pathway.

NOE Buildup Measurements for the 110-kDa Protein DHNA and the 470-kDa GroES/SR1 Complex. Experimental NOE buildup curves were obtained from multiple 2D [^{1}H,^{1}H]-NOESY experiments with DHNA and the GroES/SR1 complex, which were recorded in a series of experiments with different mixing times (Fig. 3). The $^1H^N$ assignments for DHNA were taken from Salzmann *et al.* (ref. 4; BioMagRes databank accession code 4573). Partial assignments for GroES in the complex with SR1 had been obtained by transferring sequence-specific resonance assignments from free GroES (BioMagRes databank accession code 7091) to the 2D [^{15}N,^{1}H]-CRIPT-TROSY correlation spectrum of bound GroES (14).

Fig. 3*a* shows representative NOE buildup curves for four pairs of amide protons in DHNA: The pair E66/G67 (distance $d = 2.52$ Å) shows a steep buildup curve with a short optimal mixing time of $\tau_m^o = 75$ ms. The proton pair V100/K112 ($d = 2.95$ Å) has a τ_m^o value of ≈200 ms. For G14/E16 ($d = 4.95$ Å) and I28/F29 ($d = 4.56$ Å), we have $\tau_m^o \geq 300$ ms. These observations agree qualitatively with the numerical simulations, which predicted τ_m^o values of 85, 240, 790, and 850 ms, respectively, for the amide proton pairs E66/G67, V100/K112, G14/E16, and I28/F29 (see also Fig. 2*a*).

For GroES in complex with SR1, Fig. 3*b* shows experimental NOE buildup curves for the spin pairs N2/I3, V43/G44, L57/

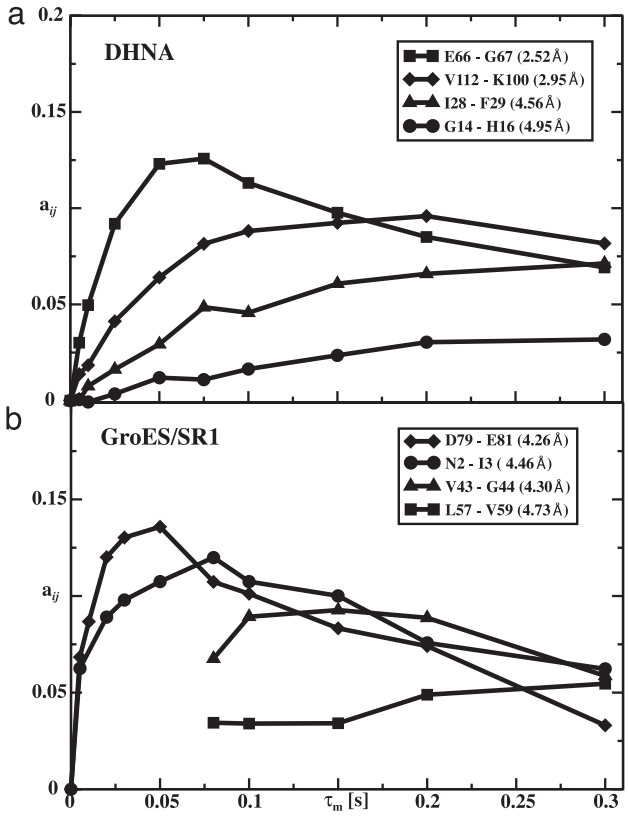

Fig. 3. Experimental NOE build-up curves. NOE transfer efficiencies, $\mathbf{a}_{ij}$, are plotted versus the mixing time, τ_m. The NOE intensities were obtained from a series of 2D ^{15}N-selected [^{1}H,^{1}H]-NOESY experiments (Fig. 5, which is published as supporting information on the PNAS web site) recorded on a Bruker Avance 900 MHz NMR spectrometer. (*a*) DHNA. (*b*) GroES in a 1:1 complex with SR1. The individual cross peak assignments and the distances between the interacting spin pairs are indicated in the figure. In *b*, the signals for V43/G44 and L57/V59 obtained for short mixing times were too weak for reliable intensity measurements.

V49, and D71/E81, which all have similar interproton distances in the range from 4.26 to 4.73 Å. The τ_m^o values vary between 50 ms and >300 ms. This wide distribution of τ_m^o values is in agreement with the simulations presented in Fig. 2*b* and mainly reflects the strong impact of spin diffusion. For the cross-peak between V43 and G44, the τ_m^o value of 170 ms obtained from the simulation (Fig. 1*a*) coincides closely with the τ_m^o value of 150 ms derived from the experimental buildup curve.

Setup of 3D ^{15}N-resolved [^{1}H,^{1}H]-NOESY Experiments with the 470-kDa SR1/GroES Complex. Sequentially neighboring amide protons have internuclear distances, d_{NN}, in the range of 2.0–4.7 Å (11). For internuclear distances <4.0 Å, the predicted τ_m^o values are between 20 and 100 ms (Fig. 2*b*). To collect all, or nearly all, of the short d_{NN} connectivities, as they occur in α-helices and some tight turns, we measured a 3D ^{15}N-resolved [^{1}H,^{1}H]-NOESY data set of GroES/SR1 with a mixing time of 100 ms. Using the model of GroES described in *Materials and Methods*, we predicted that for the amide proton pairs with $d_{NN} < 40$ Å, >90% of the peaks should have $\mathbf{a}_{ij}$ values >0.1, and should therefore be detectable in an experiment with $\tau_m = 100$ ms. In contrast, for $d_{NN} > 5.0$ Å, all $\mathbf{a}_{ij}$ values are predicted to be well below 0.1, and therefore too weak to be detected (see also Fig. 2). Therefore, we do not expect to see all of the d_{NN} connectivities in the regular β-strands with this strategy.

Resonance Assignments for GroES in the Complex with SR1. As a starting point for obtaining resonance assignments for GroES from NMR data recorded with the 470-kDa SR1/GroES complex, a 3D ^{15}N-resolved [^{1}H,^{1}H]-NOESY spectrum of the complex of uniformly [^{15}N,^{2}H]-labeled GroES with unlabeled SR1 was acquired and processed as described in *Materials and Methods*. To extract information from this spectrum, the chemical shift positions of the 87 cross-peaks previously identified in the 2D [^{15}N,^{2}H]-CRIPT-TROSY spectrum (14) were transferred to the 3D ^{15}N-resolved [^{1}H,^{1}H]-NOESY spectrum, where they were used to define [$\omega_1(^1\mathrm{H})$, $\omega_3(^1\mathrm{H})$] strips at the corresponding ^{15}N resonance positions. The diagonal peaks and the cross-peaks in each of these strips were then picked, which resulted in the identification of 142 H^N–H^N peaks. To obtain resonance assignment for the SR1-bound GroES, these fundamental data were then supplemented with additional information. First, three NMR samples of residue-specifically ^{15}N-labeled GroES, with labels on Val, Leu, or Lys/His, respectively, in complex with unlabeled SR1 were studied, and the chemical shifts of the labeled residues were transferred from 2D [^{15}N,^{1}H]-CRIPT-TROSY spectra of these samples to the NOESY spectrum, which thus defined [$\omega_1(^1\mathrm{H})$, $\omega_3(^1\mathrm{H})$] strips at the ^{15}N shifts of Val, Leu, or Lys/His residues. The NOE information in these strips was evaluated against a list of amide proton-amide proton distances among Val, Leu, Lys, and His residues, which are <5.0 Å in the crystal structure of GroES (there were 14 short distances among the 29 Val, Leu, Lys, and His residues). Using this information with the NOESY data on the uniformly labeled GroES bound to SR1 (Fig. 4*a*), the following polypeptide segments were unambiguously assigned: L6-H7, V12-K13-K15-V83-L84, V40-L41-V43, L57-V59-K60-V61, and V73-K74. These fragments could then be slightly extended by evaluating d_{NN} distances <5.0 Å between residues in these assigned peptide fragments and all of the other residues against the experimental NOEs, leading to the additional assignments of G44, D58, Y71, G72, and I85. Fig. 4 illustrates the assignments of the residues 71–74 and 85.

Second, the assignments of free GroES (BioMagRes databank accession code 7091) were used to tentatively assign diagonal peaks and cross-peaks in the 3D [^{1}H,^{1}H]-NOESY-[^{15}N,^{1}H]-CRINEPT-HMQC (heteronuclear multiple-quantum spectroscopy) spectrum of uniformly labeled SR1-bound GroES. These cross-peaks assignments were retained for pairs of amide protons that are closer than 5.0 Å to each other in the crystal structure of the GroES–GroEL complex (18). Overall, using these two approaches, we obtained resonance assignments for 61 of the 90 residues of GroES bound to SR1. The missing assignments are due to spectral overlap or absence of the corresponding NOE cross-peaks.

Structural Interpretation of NOE Data. There are several cross-peaks in the 2D [^{15}N,^{1}H]-COSY spectrum of SR1-bound GroES, which could previously not be correlated with any of the peaks of free GroES (ref. 14; see also Fig. 6, which is published as supporting information on the PNAS web site). These peaks had been tentatively attributed to a "mobile loop region" of residues 17–34 in GroES, which would be largely affected by the complex formation (14). Based on the aforementioned resonance assignments obtained in this work for SR1-bound GroES, and using additional NOE observations on the bound GroES, these earlier, hypothetical conclusions could now be verified from experimental data recorded with the 470-kDa GroES-SR1 complex.

The chemical shift positions of the cross-peaks that are unique for the bound GroES were compared with the ^{1}H chemical shifts of the residues for which resonance assignments had been obtained (see above), and a network of NOE connectivites between assigned resonances and the peaks with unique chemical shifts in the SR1–GroES complex was established (Fig. 6).

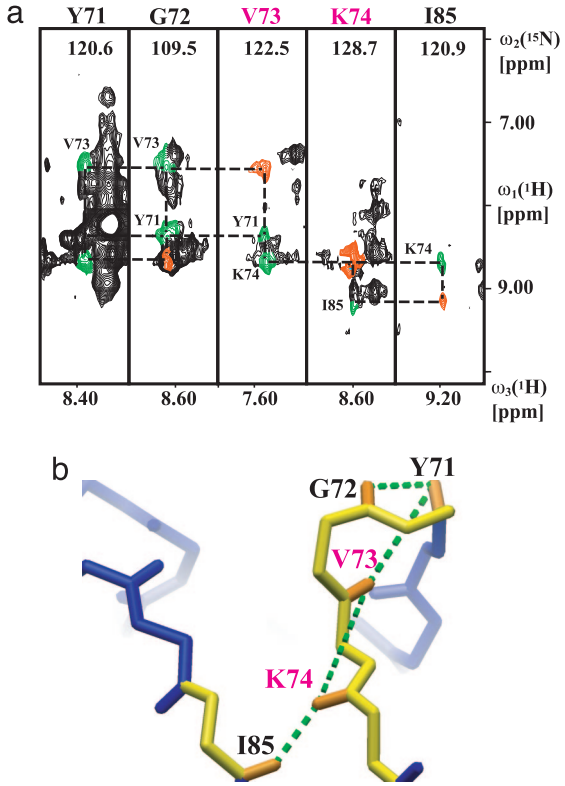

Fig. 4. Spectral and structural analysis of NMR data recorded with the GroES/SR1 complex. (*a*) [$\omega_1(^1H)$, $\omega_3(^1H)$] strips from a 3D [^1H,^1H]-NOESY-[^{15}N,^1H]-CRINEPT-HMQC spectrum of the GroES/SR1 complex. The spectrum was recorded at $T = 25°C$ using a Bruker Avance 900 NMR spectrometer (see *Supporting Text* for the experimental scheme used). The mixing time τ_m was 100 ms, the data size was $64(t_1) \times 20(t_2) \times 1,024(t_3)$ complex points, $t_{1max} = 5.1$ ms, $t_{2max} = 6.2$ ms, $t_{3max} = 81.1$ ms, and 136 scans per increment were acquired in a total measuring time of 6 days. The spectrum was processed with the program PROSA (47). Strips from the backbone amide protons 71–74 and 85 are shown. Sequence-specific resonance assignments are indicated by the one-letter amino acid code above each strip, and magenta letters indicate residues where the amino acid type was determined by residue-specific ^{15}N labeling. The direct correlation peaks and the assigned cross-peaks for each residue are marked in orange and green, respectively. The ^{15}N chemical shifts are indicated at the top of the strips. (*b*) Close-up view of the structural fragment of GroES in the complex with SR1 (18) that gives rise to the data presented in *a*. The assigned residues are highlighted in yellow and orange, and the distances d_{NN} observed in the NOESY spectrum are shown by the green dotted lines.

The combination of all these data shows that at least one of the unique NMR peaks in SR1-bound GroES originates from a residue outside of the loop 17–34, i.e., L41. Furthermore, there is a cluster of NOE connectivities between unique peaks of the bound GroES and E18, K34, and S35 at both ends of the mobile loop, indicating close approach of the two ends of the loop. These observations would appear to be compatible with the crystal structure of the GroES/GroEL/ADP complex (18), with NMR studies of the loop residues 19–27 in a synthetic peptide bound to GroEL (16, 17, 30), and with molecular dynamics simulations (17), which all indicate that the mobile loop of free GroES adopts a β-hairpin-like conformation in the complex with GroEL.

In conclusion, the principal message of this work is that NOE spectroscopy can be applied with macromolecular systems up to at least 500 kDa in size. Simulations of NOE transfers show that the maximal transfer is practically independent of the size of the protein and provide guidelines for the setup and analysis of heteronuclear-resolved [^1H,^1H]-NOESY experiments for very large deuterated proteins. For practical use, a combination of NOESY data on uniformly and amino acid-specifically ^{15}N-labeled GroES in complex with SR1 was used to assign several polypeptide segments of the bound GroES. These resonance assignments provided a platform for a structural analysis of longer-range NOEs originating from the SR1–GroES interface. This assignment approach could be extended by addition of further experiments with different selective isotope-labeling strategies.

Materials and Methods

Numerical Simulations of NOE Buildup Curves. NOESY buildup calculations were performed using a diagonalization scheme that determines eigenvalues and eigenvectors of the dynamic matrix **D** (31, 32). With the use of eigenvalues and eigenvectors, Eq. **6** takes the form in Eq. **12**

$$\mathbf{a}_{ij}(\tau_m) = [\mathbf{X}\cdot\exp\{-\mathbf{\Lambda}\tau_m\}\cdot\mathbf{X}^{-1}]_{ij}. \qquad [12]$$

X is the matrix containing the eigenvectors of **D**, and the diagonal matrix **Λ** contains the eigenvalues of the system. Numerical values for **D** (Eq. **4**) were obtained by calculating the relaxation submatrices with Eqs. **2** and **3** for a spectrometer frequency of 900 MHz, and by computing the kinetic matrix, $\mathbf{K}_B$, at pH 6.5 using a common exchange rate of $k_B = 150\ s^{-1}$ for all group B protons. The matrices **X** and **Λ** were determined by using the "QL algorithm" (33), and the $\mathbf{a}_{ij}(\tau_m)$ values were calculated with Eq. **12**. The NOESY buildup curves, $\mathbf{a}_{ij}(\tau_m)$ and τ_m^o were then calculated by using scripts written in C++, which were executed within the NMR simulation software package GAMMA (34). The output of the simulations was analyzed and displayed by using the program XMGRACE (http://plasma-gate.weizmann.ac.il).

NOESY buildup simulations were performed for three oligomeric proteins. The DHNA from *Staphylococcus aureus* is a 110-kDa homo-octamer with 121 amino acid residues per subunit (19). The cochaperonin GroES from *Escherichia coli* is a 72-kDa homo-heptamer with 97 amino acid residues per subunit (18, 35), which was studied in 1:1 complexes with SR1 and GroEL. GroEL is an 800-kDa homotetradecamer with 417 amino acids per subunit (36), with the 14 subunits arranged in two heptamer rings (37). SR1 is a single-ring heptamer variant of GroEL (38), with a molecular mass of 400 kDa. Proton–proton distances were generated from the crystal structure atom coordinates of DHNA [Protein Data Bank (PDB) ID code 1DHN], and of GroES in the GroES/GroEL complex (PDB ID code 1AON), using the program MOLMOL (39). In the simulations, we assumed complete deuteration of the CH_n groups, and complete protonation of the backbone and side chain amide groups.

NMR Sample Preparation. NMR experiments were recorded with the following two protein solutions in 95% H_2O/5% D_2O: (*i*) [u-^{15}N; u-85% ^2H]-labeled DHNA at pH 6.5, concentration 0.5 mM (4 mM per subunit), 75 mM deuterated ammonium acetate, $T = 20°C$ (4); (*ii*) [u-^{15}N, u-95% ^2H]-labeled GroES bound to unlabeled SR1 at pH 6.1, concentration 0.15 mM of the 1:1 GroES/SR1 complex (1 mM per GroES subunit), 25 mM potassium phosphate, 20 mM KCl, $T = 25°C$ (14).

Three GroES preparations with residue-specific ^{15}N-labeling complexed with unlabeled SR1 were used to support sequence-specific assignments: [^{15}N,^2H-Val, u-^2H]-GroES, [^{15}N,^2H-Leu, u-^2H]-GroES, and [^{15}N,^2H-Lys/His, u-^2H]-GroES (40).

NMR Spectroscopy. In the pulse scheme for the 2D ^{15}N-edited [^1H,^1H]-NOESY experiment used for the measurement of the NOE buildup (Fig. 5), signals from the unlabeled SR1 in the GroES/SR1 complex were suppressed by a ^{15}N-editing element

before the proton acquisition. The ^{15}N-editing was based on a CRINEPT-HMQC element (41, 42), which was combined with WATERGATE to suppress the residual solvent resonance (43) without prolonging the experimental scheme, and where the CRINEPT magnetization transfer mechanism supports efficient ^{15}N filtering (41). The optimal ^{1}H-to-^{15}N transfer period in the HMQC step was determined from 1D CRINEPT-buildup experiments (41). After each proton pulse the water was flipped back to the positive z axis to avoid signal loss due to saturation transfer from the water to the protein (27, 44).

For structural studies of the SR1-GroES complex, we used a 3D [^{1}H,^{1}H]-NOESY-[^{15}N,^{1}H]-CRINEPT-HMQC experiment (Fig. 6) with a ^{15}N evolution period in the HMQC-CRINEPT step. Because we used a short maximal evolution time, $t_{1,\max}$, and a comparatively long mixing time, τ_m, radiation damping brings the water magnetization back to equilibrium at the end of τ_m; implementing a 45° phase difference between the first two 90° ^{1}H pulses ascertains identical efficiency of radiation damping in all scans (45, 46). All NMR measurements were performed on a Bruker Avance 900 spectrometer equipped with a triple-resonance probehead with an actively shielded z-gradient coil, and the data were processed by using the program PROSA (47). The spectra were analyzed with the program XEASY (48).

We thank Dr. J. R. Williamson for helpful discussions. This work was supported by the Schweizerischer Nationalfonds and Eidgenössische Technische Hochschule Zürich through the National Centre of Competence in Research Structural Biology, the Howard Hughes Medical Institute, and the National Institutes of Health. K.W. is the Cecil H. and Ida M. Green Visiting Professor and a member of the Skaggs Institute for Chemical Biology at The Scripps Research Institute.

1. Tugarinov V, Muhandiram R, Ayed A, Kay LE (2002) *J Am Chem Soc* 124:10025–10035.
2. Fernandez C, Adeishvili K, Wüthrich K (2001) *Proc Natl Acad Sci USA* 98:2358–2363.
3. Kay LE (2005) *J Magn Reson* 173:193–207.
4. Salzmann M, Pervushin K, Wider G, Senn H, Wüthrich K (2000) *J Am Chem Soc* 122:7543–7548.
5. Salzmann M, Pervushin K, Wider G, Senn H, Wüthrich K (1998) *Proc Natl Acad Sci USA* 95:13585–13590.
6. Salzmann M, Wider G, Pervushin K, Wüthrich K (1999) *J Biomol NMR* 15:181–184.
7. Yang DW, Kay LE (1999) *J Biomol NMR* 14:273–276.
8. Braun D, Wüthrich K, Wider G (2003) *J Mag Reson* 165:89–94.
9. Kumar A, Ernst RR, Wüthrich K (1980) *Biochem Biophys Res Commun* 95:1–6.
10. Kumar A, Wagner G, Ernst RR, Wüthrich K (1981) *J Am Chem Soc* 103:3654–3658.
11. Billeter M, Braun W, Wüthrich K (1982) *J Mol Biol* 155:321–346.
12. Wider G, Lee KH, Wüthrich K (1982) *J Mol Biol* 155:367–388.
13. Wüthrich K, Wagner G (1979) *J Mol Biol* 130:1–18.
14. Fiaux J, Bertelsen EB, Horwich AL, Wüthrich K (2002) *Nature* 418:207–211.
15. Hunt JF, Weaver AJ, Landry SJ, Gierasch L, Deisenhofer J (1996) *Nature* 379:37–45.
16. Landry SJ, Zeilstraryalls J, Fayet O, Georgopoulos C, Gierasch LM (1993) *Nature* 364:255–258.
17. Shewmaker F, Maskos K, Simmerling C, Landry SJ (2001) *J Biol Chem* 276:31257–31264.
18. Xu ZH, Horwich AL, Sigler PB (1997) *Nature* 388:741–750.
19. Hennig M, D'Arcy A, Hampele IC, Page MGP, Oefner C, Dale GE (1998) *Nat Struct Biol* 5:357–362.
20. Stoesz JD, Redfield AG, Malinowski D (1978) *FEBS Lett* 91:320–324.
21. Akasaka K, Konrad M, Goody RS (1978) *FEBS Lett* 96:287–290.
22. Dill K, Huang LH, Bearden DW (1992) *J Biomol NMR* 2:173–181.
23. Landy SB, Rao BDN (1989) *J Mag Reson* 83:29–43.
24. Solomon I (1955) *Phys Rev* 99:559–565.
25. Goldman M (1984) *J Mag Reson* 60:437–452.
26. Kumar A, Grace RCR, Madhu PK (2000) *Prog Nucl Magn Reson Spectrosc* 37:191–319.
27. Grzesiek S, Bax A (1993) *J Am Chem Soc* 115:12593–12594.
28. Macura S, Ernst RR (1980) *Mol Phys* 41:95–117.
29. Blatter C (1991) *Analysis* (Springer, Heidelberg).
30. Landry SJ, Taher A, Georgopoulos C, van der Vies SM (1996) *Proc Natl Acad Sci USA* 93:11622–11627.
31. Forster MJ (1991) *J Comput Chem* 12:292–300.
32. Keepers JW, James TL (1984) *J Mag Reson* 57:404–426.
33. Press WH, Teukolsky SA, Vetterling WT, Flannery BP (1988) *Numerical Recipes in C*: *The Art of Scientific Computing* (Cambridge Univ Press, Cambridge, UK).
34. Smith SA, Levante TO, Meier BH, Ernst RR (1994) *J Magn Reson Ser A* 106:75–105.
35. Chandrasekhar GN, Tilly K, Woolford C, Hendrix R, Georgopoulos C (1986) *J Biol Chem* 261:2414–2419.
36. Hemmingsen SM, Woolford C, Vandervies SM, Tilly K, Dennis DT, Georgopoulos CP, Hendrix RW, Ellis RJ (1988) *Nature* 333:330–334.
37. Braig K, Otwinowski Z, Hedge R, Boisvert DC, Joachimiak A, Horwich AL, Sigler PB (1994) *Nature* 371:578–586.
38. Weissman JS, Rye HS, Fenton WA, Beechem JM, Horwich AL (1995) *Cell* 83:577–587.
39. Koradi R, Billeter M, Wüthrich K (1996) *J Mol Graphics* 14:51–56.
40. Fiaux J, Bertelsen EB, Horwich AL, Wüthrich K (2004) *J Biomol NMR* 29:289–297.
41. Riek R, Wider G, Pervushin K, Wüthrich K (1999) *Proc Natl Acad Sci USA* 96:4918–4923.
42. Bodenhausen G, Ruben DJ (1980) *Chem Phys Lett* 69:185–189.
43. Piotto M, Saudek V, Sklenar V (1992) *J Biomol NMR* 2:661–665.
44. Hiller S, Wider G, Etezady-Esfarjani T, Horst R, Wüthrich K (2005) *J Biomol NMR* 32:61–70.
45. Lippens G, Dhalluin C, Wieruszeski JM (1995) *J Biomol NMR* 5:327–331.
46. Talluri S, Wagner G (1996) *J Magn Reson Ser B* 112:200–205.
47. Güntert P, Dötsch V, Wider G, Wüthrich K (1992) *J Biomol NMR* 2:619–629.
48. Bartels C, Xia TH, Billeter M, Güntert P, Wüthrich K (1995) *J Biomol NMR* 6:1–10.
49. Wagner G, Wüthrich K (1979) *J Magn Reson* 55:151–156.
50. Salzmann M, Wider G, Pervushin K, Senn H, Wüthrich K (1999) *J Am Chem Soc* 121:844–848.
51. Riek R, Fiaux J, Bertelsen EB, Horwich AL, Wüthrich K (2002) *J Am Chem Soc* 124:12144–12153.